Research Square

Preprints are preliminary reports that have not undergone peer review.
They should not be considered conclusive, used to inform clinical practice,
or referenced by the media as validated information.

α-Synuclein drives intracellular acidification by preventing lysosomal degradation of the anion exchanger AE2

Fabio Falleroni

fabio.falleroni@aomliguria.it

IRCCS Azienda Ospedaliera Metropolitana (IRCCS AOM) Plesso: Ospedale Policlinico San Martino

Lorenzo Mazzola

University of Genoa

Martina Pasino

IRCCS Azienda Ospedaliera Metropolitana (IRCCS AOM) Plesso: Ospedale Policlinico San Martino

Alessio Cirone

IRCCS Azienda Ospedaliera Metropolitana (IRCCS AOM) Plesso: Ospedale Policlinico San Martino

Federico Carlini

IRCCS Azienda Ospedaliera Metropolitana (IRCCS AOM) Plesso: Ospedale Policlinico San Martino

Michela Chiappalone

University of Genoa

Antonio Uccelli

IRCCS Azienda Ospedaliera Metropolitana (IRCCS AOM) Plesso: Ospedale Policlinico San Martino

Sergio Martinoia

University of Genoa

Article

Keywords:

Posted Date: May 18th, 2026

DOI: https://doi.org/10.21203/rs.3.rs-9618156/v1

License: This work is licensed under a Creative Commons Attribution 4.0 International License.
Read Full License

Additional Declarations: (Not answered)

Abstract

α-Synuclein (α-Syn) accumulation is a central pathological feature of Parkinson's disease, yet its impact extends beyond proteostasis failure. Here, we identify intracellular pH dysregulation as a previously unrecognized consequence of α-Syn overexpression in neuronally differentiated SH-SY5Y cells. α-Syn promotes cytosolic acidification by stabilizing the acid-loading anion exchanger AE2 (SLC4A2) through mTOR-dependent impairment of lysosomal degradation. Pharmacological modulation of this pathway revealed opposite effects on AE2 turnover: rapamycin rescued, whereas bafilomycin A1 exacerbated, AE2 accumulation, in parallel with reciprocal changes in intracellular pH (alkalinization with rapamycin and further acidification with bafilomycin). Because acidic conditions favor misfolding and aggregation of this intrinsically disordered protein, α-Syn–driven acidification may establish a self-reinforcing pathogenic loop that fuels disease progression. Our findings identify AE2-mediated acid loading as a central driver of α-Syn–induced cellular dysfunction, establishing intracellular pH dysregulation as a possible core pathogenic mechanism in synucleinopathies.

Introduction

Parkinson's disease (PD) is a progressive neurodegenerative disorder defined by the aberrant accumulation of misfolded α-synuclein (α-Syn) and the selective loss of dopaminergic neurons (1). Although α-Syn aggregation is recognized as a central pathological hallmark, the mechanisms linking protein misfolding to neuronal dysfunction remain incompletely understood.

Over the past decade, increasing evidence has shown that α-Syn pathology extends beyond protein aggregation and affects multiple aspects of cellular homeostasis. α-Syn interferes with proteostasis, vesicular trafficking, and lysosomal degradation, functions that are essential to maintain cellular balance (2). Among these, lysosomal impairment has emerged as a key contributor to PD progression, supported by genetic evidence linking lysosomal genes to disease risk and by functional studies indicating defective autophagic flux in α-Syn models (3). Yet how these degradative and trafficking defects converge on the fundamental physicochemical parameters that govern cell physiology remains unclear.

Intracellular pH (pH_i) is one such parameter. Tightly regulated, pH_i orchestrates enzymatic activity, ion transport, organellar communication, and degradation pathways (4). Neurons, with their polarized morphology and high metabolic demands, are particularly sensitive to variations in pH_i since even small, acid–base fluctuations can alter excitability, vesicle recycling, and cell survival (5). Despite its functional importance, how α-Syn influences neuronal pH regulation and whether changes in pH_i contribute to its toxicity remain largely unknown.

Maintenance of pH_i relies on the coordinated activity of multiple membrane channels and intracellular organelles. Surface-expressed transporters act as the primary gatekeepers of pH_i, as they export excess acid or base into the extracellular space. Acid extruders — including the Na^+/H^+ exchanger NHE1 (SLC9A1), monocarboxylate transporters (MCTs), and Na^+/HCO_3^- co-transporters (NBCs) — are the

predominant regulators of cytosolic alkalinization. However, steady-state pHi is not determined by extrusion alone: acid loaders, particularly the Na^+-independent Cl^-/HCO_3^- exchangers of the SLC4 family (AE1–3). Together, these opposing transport systems, in concert with lysosomal proton sequestration via the V-ATPase, maintain cytosolic pH within a narrow physiological range (6). Since anion exchangers contribute to steady-state pHi by balancing the activity of acid extruders, disruption of this equilibrium — whether through enhanced extrusion or suppressed acid loading — can precipitate pathological cytosolic alkalinization and metabolic stress. A key upstream regulator of lysosomal function and metabolic homeostasis is the mechanistic target of rapamycin (mTOR), which integrates nutrient and stress signals to coordinate lysosomal biogenesis and autophagy (7). Dysregulation of mTOR signalling has been consistently reported in PD models and patient tissues (8), where it correlates with impaired lysosomal activity and incomplete autophagic clearance. Pathological α-Syn can activate mTOR (9, 10), suggesting a reciprocal relationship between proteostatic failure and metabolic imbalance. However, whether mTOR-dependent pathways contribute to pH_i alterations and whether such effects amplify α-Syn toxicity remain unexplored.

Here we show that pathological α-Syn expression induces cytosolic acidification by stabilizing the acid-loading exchanger AE2 through mTOR-dependent lysosomal dysfunction. These findings identify pH dysregulation as a previously unrecognized axis of α-Syn toxicity and position pH homeostasis as a potential therapeutic target in Parkinson's disease.

Results

Pathological α-Synuclein induces intracellular acidification in SH-SY5Y cells

To validate α-synuclein (α-Syn) overexpression, we compared wild-type (WT) and 3K-SNCA (SNCA) SH-SY5Y cells using immunofluorescence and Western blot analyses. Both approaches showed a marked increase in cytosolic α-Syn signal intensity in SNCA cells relative to WT controls, confirming the robustness of the overexpression model (Fig. 1A-C).

Intracellular pH (pHi) was then measured using the ratiometric fluorescent probe BCECF-AM, calibrated with the standard nigericin/high-K^+ method (Fig. 1D). Ratiometric imaging revealed a consistent reduction of pH_i values in α-Syn-overexpressing cells compared with WT controls (Fig. 1E), indicating global cytosolic acidification. Quantitative analysis showed that WT cells maintained a mean pHi of 7.07 ± 0.19, whereas SNCA cells displayed a significantly lower mean pHi of 6.84 ± 0.14 (Fig. 1F). Notably, the shift of the entire pHi distribution indicates a uniform decrease across the cell population rather than the emergence of discrete subpopulations.

Together, these findings demonstrate that pathological α-Syn accumulation is sufficient to drive homogeneous intracellular acidification, establishing altered pH homeostasis as a direct and global consequence of α-Syn expression.

AE2, rather than NHE1, dominates steady-state intracellular pH control under α-synuclein expression

Basal pHi is maintained by the coordinated activity of proton extruders and bicarbonate-dependent exchangers. To dissect which mechanisms shape pHi under α-Syn expression, we focused on the Na^+/H^+ exchanger NHE1 and the anion exchanger AE2.

Pharmacological inhibition of NHE1 with cariporide induced only a modest acidification in both wild-type (WT) and SNCA cells (Fig. 2B and C), indicating that NHE1 contributes to basal proton extrusion but has a limited impact on the α-Syn–associated acidification phenotype.

To assess the net direction of bicarbonate-dependent transport, we removed HCO_3^- by switching from CO_2/HCO_3^- buffer to HEPES. If HCO_3^--dependent transporters primarily mediated acid extrusion, substrate removal would be expected to induce acidification; instead, both WT and SNCA cells underwent alkalinization, indicating that the dominant direction of HCO_3^--dependent flux is acid loading. Notably, this alkalinization was more pronounced in SNCA cells compared to WT controls (Fig. 2B–E).

These findings indicate that bicarbonate-dependent transport exerts a strong acid-loading influence on steady-state pHi, which is enhanced under α-Syn expression. The exaggerated alkalinization observed upon HCO_3^- removal in SNCA cells suggests increased activity of acid-loading transporters, consistent with a predominant role for the anion exchanger AE2 in driving cytosolic acidification.

Together, these results identify AE2-mediated acid loading as a dominant determinant of intracellular pH and implicate its pathological upregulation as a key mechanism underlying the acidification phenotype associated with α-Syn accumulation.

α-Synuclein drives alterations in anion exchanger expression and compromises lysosomal function

To investigate the mechanisms underlying pHi dysregulation in SNCA cells, we examined whether α-Syn expression is associated with changes in anion exchanger (AE2) expression and lysosomal function.

Immunofluorescence revealed a marked increase in AE2 signal intensity in SNCA cells compared to wild-type (WT) controls, accompanied by a more diffuse cytoplasmic distribution (Fig. 3A). Quantitative single-cell analysis confirmed significantly elevated AE2 levels in SNCA cells relative to WT (Fig. 3B), indicating that α-synuclein accumulation is related to AE2 upregulation.

Inhibition of lysosomal acidification with bafilomycin A1 further increased AE2 levels in both WT and SNCA cells, with a comparatively stronger effect in WT cells (Fig. 3C). This differential response likely reflects the higher basal AE2 expression already present in SNCA cells. Collectively, these findings indicate that AE2 turnover is lysosome-dependent and that its accumulation results from impaired lysosomal degradation.

Live-cell imaging with Lysobright Green revealed a marked reduction in lysosomal fluorescence in SNCA cells compared to WT (Fig. 3D). Quantitative analysis confirmed a decrease in both the number and intensity of lysosomal structures, consistent with impaired lysosomal acidification and reduced lysosomal content (Fig. 3E).

Assessment of autophagy markers by Western blot further supported lysosomal impairment. SNCA cells displayed elevated p62/SQSTM1 levels (1.2 ± 0.15 fold of control vs 0.65 ± 0.1 in WT) together with a reduced LC3-II/LC3-I ratio (0.85 ± 0.1 fold of control vs 1.4 ± 0.15 in WT) (Fig. 3F), a pattern consistent with blocked autophagic flux and accumulation of autophagic intermediates.

To summarize, these findings indicate that α-synuclein accumulation is accompanied by lysosomal dysfunction, characterized by reduced lysosomal abundance and impaired degradative capacity. In this context, diminished lysosomal turnover favors the stabilization of AE2 at the plasma membrane, thereby promoting sustained cytosolic acidification in SNCA cells.

Inhibition of mTOR restores pHi through increased lysosomal activity and AE2 turnover

Given the lysosomal dysfunction and AE2 accumulation observed in SNCA cells, we next investigated whether aberrant activation of the mechanistic target of rapamycin (mTOR) pathway contributes to these defects. As a central regulator of lysosomal biogenesis and autophagic flux, mTOR represents a key candidate linking impaired lysosomal function to defective protein turnover and pH dysregulation.

Western blot analysis revealed elevated levels of phosphorylated mTOR (p-mTOR) in SNCA cells relative to wild-type (WT) controls (Fig. 4A consistent with enhanced mTOR pathway activation under α-synuclein overexpression.

To test whether mTOR activity affects intracellular pH (pHi), we targeted mTORC1, the complex responsible for lysosomal and autophagic regulation, using its selective inhibitor rapamycin. Fluorescence analysis revealed a strong negative modulation of AE2 expression, with SNCA cells showing a greater reduction than WT cells (Fig. 4C). Moreover, the inhibition of lysosomal function by bafilomycin A1 decreased pHi in both WT and SNCA cells, reflecting impaired lysosomal proton sequestration. Conversely, rapamycin treatment shifted the distribution toward higher pH values, restoring a more neutral cytosolic environment, especially in SNCA cells (Fig. 4B and D).

Single-cell quantification confirmed these effects (Fig. 4E–F). Treatment with bafilomycin A1 further exacerbated cytosolic acidification in both WT and SNCA cells, whereas rapamycin induced a marked alkalinization. Notably, rapamycin largely restored pHi in SNCA cells, reducing the difference between WT and SNCA populations.

These findings identify mTOR signaling as a key determinant of pHi homeostasis. Overactive mTOR in SNCA cells likely contributes to defective lysosomal acidification and insufficient AE2 turnover, leading to persistent cytosolic acidification. Inhibition of mTORC1 reactivates autophagic flux, thereby promoting lysosomal clearance and accelerating AE2 turnover, effects that collectively re-establish physiological pH balance and identify mTOR as a central regulator of the acid–base alterations associated with α-synuclein pathology.

Discussion

The present study identifies intracellular pH dysregulation as a previously unrecognized functional consequence of pathological α-synuclein accumulation. Our data show that α-synuclein stabilizes the acid-loading anion exchanger AE2 through mTOR-dependent impairment of lysosomal degradation, thereby linking proteostatic dysfunction directly to cytosolic acidification.

Prior studies on pH regulation in neurodegeneration have focused predominantly on defective proton extrusion. Endosomal NHE6 and NHE9 have been implicated in Alzheimer's disease and autism spectrum disorder through dysregulation of endosomal pH and vesicular trafficking (13), and members of the NHE family have been proposed as modifiers of neuronal vulnerability in Parkinson's disease (11, 12). By contrast, our findings shift this perspective by identifying enhanced acid loading, rather than impaired proton extrusion, as the main driver of cytosolic acidification. Pharmacological dissection demonstrated that inhibition of AE2-mediated bicarbonate exchange, rather than NHE1 blockade, accounted for most of the pHi variation observed in SNCA-expressing cells. This distinction carries significant mechanistic weight: unlike proton extrusion, which consumes ATP and may be further compromised in metabolically stressed neurons, AE2-driven acid loading operates independently of energetic state, making it a persistent and self-reinforcing source of cytosolic acidification in neurodegenerative settings.

Notably, our data place lysosomal dysfunction at the center of this mechanism. α-Syn accumulation is associated with reduced lysosomal abundance and impaired degradative capacity, conditions that are expected to limit the turnover of membrane proteins. In this context, defective lysosomal clearance promotes the stabilization of AE2 at the plasma membrane, thereby amplifying acid-loading activity. This identifies lysosomes not only as targets of α-Syn toxicity, but also as key regulators of pH homeostasis through their control of transporter turnover. The marked reduction in lysosomal signal observed in SNCA cells, together with elevated p62 and a reduced LC3-II/LC3-I ratio, is consistent with previous reports of impaired autophagy–lysosomal pathway activity in α-synuclein models (3), and extends these findings by identifying AE2 stabilization and intracellular acid loading as direct functional consequences of this degradative failure.

The rescue achieved by rapamycin-mediated mTORC1 inhibition is particularly informative in this context. The preferential recovery of pHi observed in SNCA cells after rapamycin treatment indicates that mTOR hyperactivation is the primary signal maintaining lysosomal dysfunction. This is consistent with reports that pathological α-synuclein disrupts the TSC1–TSC2 complex to sustain mTORC1 activity and with the broader literature linking mTOR dysregulation to impaired lysosomal biogenesis and autophagic clearance in patient tissues (8–10). Restoration of AE2 turnover following mTORC1 inhibition further supports the conclusion that reactivation of autophagic flux is sufficient to normalize intracellular acid balance.

A particularly important feature of the mechanism described here is its capacity for self-amplification. α-Syn is an intrinsically disordered protein (IDP) whose aggregation propensity is strongly modulated by pH: acidic conditions promote the conformational transitions that favor β-sheet formation and amyloid

nucleation (15, 16). The cytosolic acidification induced by AE2 stabilization may therefore accelerate α-synuclein misfolding, establishing a feed-forward cycle in which the protein enhances its own aggregation through a pH-dependent mechanism. This cycle would be expected to intensify over time, as progressive aggregation further impairs lysosomal function, further limits AE2 clearance, and further depresses pHi. Whether this amplification operates in vivo, and whether it contributes to the stereotyped propagation of α-synuclein pathology observed in Parkinson's disease, are questions that warrant direct investigation in primary neurons and animal models.

Beyond its effects on proteostasis, the cytosolic acidification described here carries specific functional implications for dopaminergic neurotransmission. Tyrosine hydroxylase, the rate-limiting enzyme in dopamine biosynthesis, exhibits strong pH dependence: its catalytic efficiency and substrate affinity are optimal at neutral to mildly alkaline pH, and even modest reductions below pH 7.0 significantly impair its activity (17). The cytosolic acidification observed in SNCA cells falls within a range that would be expected to compromise tyrosine hydroxylase function, suggesting that α-synuclein-driven acidification may contribute to dopamine synthesis deficits before overt neuronal loss occurs. In addition, vesicular monoamine transporter 2 (VMAT2), which relies on the vesicular proton gradient to concentrate dopamine within synaptic vesicles, may also be functionally altered in an acidified cytosolic environment, further disturbing dopamine storage and release. Together, these considerations suggest that intracellular acidification may represent an early mechanism of dopaminergic dysfunction in Parkinson's disease — one that precedes and likely amplifies the neurodegenerative cascade. Directly testing this hypothesis, through measurement of tyrosine hydroxylase activity and dopamine synthesis rates across overexpressing α-Syn cells, represents an important priority for future work.

The mechanistic framework emerging from this study identifies several therapeutically tractable nodes. mTORC1 inhibition with rapamycin restored both AE2 turnover and pHi in SNCA cells, providing proof-of-concept that reactivating autophagic flux is sufficient to partially normalize cytosolic acid balance. While chronic rapamycin use carries well-documented immunosuppressive liabilities, next-generation mTORC1-selective inhibitors may offer a more favorable therapeutic window (18). Alternatively, direct modulation of AE2 activity or pharmacological activation of TFEB to promote lysosomal reacidification could simultaneously enhance AE2 clearance and proton sequestration capacity. (19). Given the pH dependence of α-syn aggregation, even partial pHi restoration may be sufficient to interrupt the feed-forward cycle linking acidification to proteostatic collapse, a prediction that should now be tested in primary dopaminergic neurons and in vivo models of Parkinson’s disease.

Materials and Methods

Cell culture and generation of SNCA-overexpressing cells

Human neuroblastoma cells SH-SY5Y (ATCC number: CRL-2266) and 3K-SNCA cells were maintained at 37 °C in a humidified atmosphere with 5% CO_2. Cells were initially cultured in Dulbecco’s Modified Eagle Medium/Nutrient Mixture F-12 (DMEM/F12) supplemented with 10% fetal bovine serum (FBS), 1%

penicillin–streptomycin, and GlutaMAX. After 24 h, cells were switched to Neurobasal medium supplemented with B27, GlutaMAX, and 1% penicillin–streptomycin (Neuronal complete medium, NCM) to promote neuronal differentiation for 8 DIV.

pH ratiometric live imaging

Intracellular pH (pH_i) was measured using the ratiometric fluorescent probe BCECF-AM (Thermo Fisher Scientific, #B1170). Cells were loaded with BCECF-AM at a final concentration of 5 µM for 30 min at 37 °C in neuronal complete medium (NCM). After loading, cells were washed and imaged in NCM or HEPES-buffered low-chloride solution, depending on the experimental condition.

Calibration of BCECF fluorescence was performed using the nigericin/high-K^+ equilibration method. Briefly, cells were incubated in calibration buffers of defined pH values (range 5.5–8.5) containing high potassium and nigericin (20 µM) to equilibrate intracellular and extracellular pH. Fluorescence emission ratios (488/440 nm) were measured and plotted against the corresponding buffer pH values to generate a calibration curve.

To convert fluorescence ratios (R) into absolute intracellular pH values, data were fitted using a modified Henderson–Hasselbalch equation derived from the calibration curve:

$$pH = 7.07 - \log_{10}\left(\frac{2.10 - R}{R - 0.41}\right)$$pH=7.07−log10(R−0.412.10−R)

where *R* represents the fluorescence ratio (488/440 nm), and constants were determined experimentally from calibration parameters.

Pharmacological treatments

To modulate pH-regulatory pathways, cells were treated with specific pharmacological or buffering conditions prior to intracellular pH measurements. Inhibition of the Na^+/H^+ exchanger NHE1 was achieved by pre-incubating cells with cariporide (30 M). To inhibit anion exchanger (AE2) activity and eliminate CO2/HCO3-dependent buffering, cells were incubated were incubated in Live Cell Imaging Solution (Thermo Fisher Scientific, catalog no. A59688DJ), a HEPES-buffered, CO_2-independent medium. For lysosomal and mTOR modulation, cells were treated with bafilomycin A1 (10 nM), an inhibitor of the vacuolar H^+-ATPase, or with rapamycin (10 nM), a selective inhibitor of mTOR. Treatments were performed in neuronal complete medium (NCM) for 72 h prior to experimental measurements. All treatments were performed under identical conditions for WT and SNCA cells.

Western blot analysis

Cells were lysed in ice-cold RIPA buffer supplemented with protease and phosphatase inhibitors (Thermo Fisher Scientific, #78440). g of total proteins were separated by SDS-PAGE on a 4-15% Mini Protean TGX precast gel (Bio-Rad, Milan, Italy) and transferred to nitrocellulose membranes using Trans-

Blot Turbo Blotting System. Membranes were blocked for 2 h in 2% Bovine Serum Albumin (BSA) prepared in 0.1% Tween-20 in PBS 1X and incubated overnight at ﷺ or 1 h at room temperature with primary antibodies against ﷺ-synuclein (Proteintech, #10842-1-AP 1:1000),phosphorylated mTOR (Ser2448; Cell Signaling Technology, #5536; 1:1000), SQSTM1/p62 (Cell Signaling Technology, #5114; 1:500), LC3B (Novus Biologicals, NB600-1384, 1:1000) and loading control GAPDH (14C10; Cell Signaling Technology, #2118; 1:1000). Membranes were then incubated with IgG-horseradish peroxidase-conjugated secondary antibody anti-rabbit HRP (A9169, Sigma-Aldrich, 1:12,000). After incubation, immunoreactive bands were detected using Pierce ECL Western Blotting Substrate (Thermo Fisher Scientific) by Alliance LD, UVITEC Cambridge (Cambridge, UK). Chemiluminescence was quantified using ImageJ/Fiji. Original uncropped western blots are provided in Supplementary Information.

Immunofluorescence and lysosomal imaging

Cells were fixed with 4% paraformaldehyde (PFA) in phosphate-buffered saline (PBS) for 15 min at room temperature, followed by three washes in PBS. Cells were then permeabilized with 0.1% Triton X-100 in PBS for 10 min and blocked with 5% BSA in PBS for 1 h at room temperature to prevent non-specific binding.

Primary antibody incubation was performed overnight at 4°C in blocking solution. The following primary antibodies were used: anti-α-synuclein (Proteintech, #10842-1-AP 1:500), and AE2 Rabbit anti-Human (Proteintech, Cat. No. 26332-1-AP 1:200). After primary antibody incubation, cells were washed three times with PBS and incubated with fluorescently labeled secondary antibodies (Alexa Fluor-conjugated 488 nm, 1:500 dilution) for 1 h at room temperature. Nuclei were counterstained with DAPI (1 µg/mL) for 5 min.

Fluorescence images were acquired using a FV5000 confocal microscope (Evident) under identical acquisition settings, including exposure time, gain, and illumination intensity, across all experimental conditions.

Lysosomal activity was assessed by live-cell imaging using the fluorescent probe LysoBright. Cells were incubated with LysoBright 4 µM in pre-warmed culture medium for 30 min at 37 °C in a humidified incubator with 5% CO_2. After incubation, cells were washed once with fresh medium and immediately imaged. Fluorescence intensity was quantified using both Cellpose-SAM and image analysis software (ImageJ/Fiji). All acquisition and analysis parameters were kept constant across conditions, and analyses were performed blind to experimental groups.

Multi-channel images (brightfield, DAPI, and fluorescence channels) were processed using a standardized analysis pipeline to quantify fluorescence signals. Quantitative measurements were performed on raw fluorescence images, which were first processed using the RIAJ plugin in Fiji/ImageJ to generate ratio images.

Cell segmentation was then performed using Cellpose (v2.2.3), and the resulting masks were used to define individual regions of interest (ROIs). These masks were subsequently applied to the ratio images in Fiji/ImageJ to extract fluorescence intensity values. For each validated ROI, fluorescence intensity was quantified as either integrated density (IntDen) or mean intensity, depending on the analysis, providing a cell-resolved measure of signal (a schematic workflow is shown in Supplementary Fig. 1).

Data analysis and statistics

All experiments were performed with at least three independent biological replicates. Data are presented as mean ± SD unless otherwise specified. Each data point represents a single cell pooled from independent experiments or the mean of independent experiments, as indicated in the corresponding figure legends.

Statistical analyses were performed using GraphPad Prism (version 10). For comparisons between two groups, an unpaired two-tailed Student's *t*-test was used. For comparisons involving more than two groups, one-way ANOVA followed by Tukey's post hoc test was applied. When data did not meet the assumptions of normality, non-parametric tests were used as appropriate.

Statistical significance was defined as $p < 0.05$.

Limitation of study

Several limitations should be acknowledged. First, these findings are based on cellular models and require validation in primary neurons and *in vivo* systems. Second, while mTOR activation is clearly implicated, the precise molecular events linking α-Syn to mTOR remain to be fully elucidated. Third, additional ion transporters may contribute to pH regulation beyond AE2 and NHE1.

Despite these limitations, our study provides a conceptual framework that integrates mTOR signaling, lysosomal dysfunction, and intracellular pH regulation in α-Syn pathology. Importantly, the ability of mTOR inhibition to restore pH homeostasis highlights the therapeutic potential of targeting the mTOR–lysosome–pH axis. Interventions aimed at modulating intracellular pH or its regulatory mechanisms may represent a novel strategy to counteract α-Syn-induced neurotoxicity.

Declarations

Acknowledgments

We thank Simona Francia for her critical review of the manuscript and helping with the figures.

Confilct of Interests

The authors declare no competing interests.

Author Contributions

F.F. conceptualized the study. L.D.M. and M.P. performed the experiments. A.C., L.D.M. and F.F. performed computational analysis. A.U. and S.M. provided intellectual input. L.D.M., F.C. and F.F. wrote the manuscript. All authors reviewed and approved the final version.

Ethics statement

This study was conducted using established human cell lines (SH-SY5Y) and did not involve human participants or animal subjects. Ethical approval was therefore not required.

Funding statement

This study was conducted without any external funding

References

1. Calabresi P, Mechelli A, Natale G, Volpicelli-Daley L, Di Lazzaro G, Ghiglieri V. Alpha-synuclein in Parkinson's disease and other synucleinopathies: from overt neurodegeneration back to early synaptic dysfunction. Cell Death Dis. 1 marzo 2023;14(3):176. doi:10.1038/s41419-023-05672-9
2. Nachman E, Verstreken P. Synaptic proteostasis in Parkinson's disease. Curr Opin Neurobiol. febbraio 2022;72:72–9. doi:10.1016/j.conb.2021.09.001
3. Brooker SM, Naylor GE, Krainc D. Cell biology of Parkinson's disease: Mechanisms of synaptic, lysosomal, and mitochondrial dysfunction. Curr Opin Neurobiol. aprile 2024;85:102841. doi:10.1016/j.conb.2024.102841
4. Putnam RW. Intracellular pH Regulation. In: Cell Physiology Source Book [Internet]. Elsevier; 2001 [citato 1 aprile 2026]. p. 357–72. Disponibile su: https://linkinghub.elsevier.com/retrieve/pii/B9780126569766501141 doi:10.1016/B978-012656976-6/50114-1
5. Ruffin VA, Salameh AI, Boron WF, Parker MD. Intracellular pH regulation by acid-base transporters in mammalian neurons. Front Physiol. 2014;5. doi:10.3389/fphys.2014.00043
6. Aoi W, Marunaka Y. Importance of pH Homeostasis in Metabolic Health and Diseases: Crucial Role of Membrane Proton Transport. BioMed Res Int. 2014;2014:1–8. doi:10.1155/2014/598986
7. Settembre C, Perera RM. Lysosomes as coordinators of cellular catabolism, metabolic signalling and organ physiology. Nat Rev Mol Cell Biol. marzo 2024;25(3):223–45. doi:10.1038/s41580-023-00676-x
8. Crino PB. The mTOR signalling cascade: paving new roads to cure neurological disease. Nat Rev Neurol. luglio 2016;12(7):379–92. doi:10.1038/nrneurol.2016.81
9. Khan MR, Yin X, Kang SU, Mitra J, Wang H, Ryu T, et al. Enhanced mTORC1 signaling and protein synthesis in pathologic α-synuclein cellular and animal models of Parkinson's disease. Sci Transl Med. 29 novembre 2023;15(724):eadd0499. doi:10.1126/scitranslmed.add0499

10. Gao S, Duan C, Gao G, Wang X, Yang H. Alpha-synuclein overexpression negatively regulates insulin receptor substrate 1 by activating mTORC1/S6K1 signaling. Int J Biochem Cell Biol. luglio 2015;64:25–33. doi:10.1016/j.biocel.2015.03.006
11. Prasad H. Genes for endosomal pH regulators NHE6 and NHE9 are dysregulated in the substantia nigra in Parkinson's disease. Gene. novembre 2024;927:148737. doi:10.1016/j.gene.2024.148737
12. Verma V, Bali A, Singh N, Jaggi AS. Implications of sodium hydrogen exchangers in various brain diseases. J Basic Clin Physiol Pharmacol. 1 settembre 2015;26(5):417–26. doi:10.1515/jbcpp-2014-0117
13. Prasad H, Rao R. The Na+/H+ Exchanger NHE6 Modulates Endosomal pH to Control Processing of Amyloid Precursor Protein in a Cell Culture Model of Alzheimer Disease. J Biol Chem. febbraio 2015;290(9):5311–27. doi:10.1074/jbc.M114.602219
14. Chen R, Jäättelä M, Liu B. Lysosome as a Central Hub for Rewiring PH Homeostasis in Tumors. Cancers. 27 agosto 2020;12(9):2437. doi:10.3390/cancers12092437
15. Khare SD, Chinchilla P, Baum J. Multifaceted interactions mediated by intrinsically disordered regions play key roles in alpha synuclein aggregation. Curr Opin Struct Biol. giugno 2023;80:102579. doi:10.1016/j.sbi.2023.102579
16. Cho M, Nodet G, Kim H, Jensen MR, Bernado P, Fernandez CO, et al. Structural characterization of α-synuclein in an aggregation prone state. Protein Sci. settembre 2009;18(9):1840–6. doi:10.1002/pro.194
17. Daubner SC, Le T, Wang S. Tyrosine hydroxylase and regulation of dopamine synthesis. *Arch Biochem Biophys*. 2011;508(1):1–12. doi:10.1016/j.abb.2010.12.017
18. Kaur N, Bhatt LK. Novel mTORC1 inhibitors for neurodegeneration. *Drug Discov Today*. 2024;29(1):103849. doi:10.1016/j.drudis.2023.103849
19. Bonam SR, Wang F, Muller S. Lysosomes as a therapeutic target. *Nat Rev Drug Discov*. 2019;18(12):923–48. doi:10.1038/s41573-019-0036-1

Figures

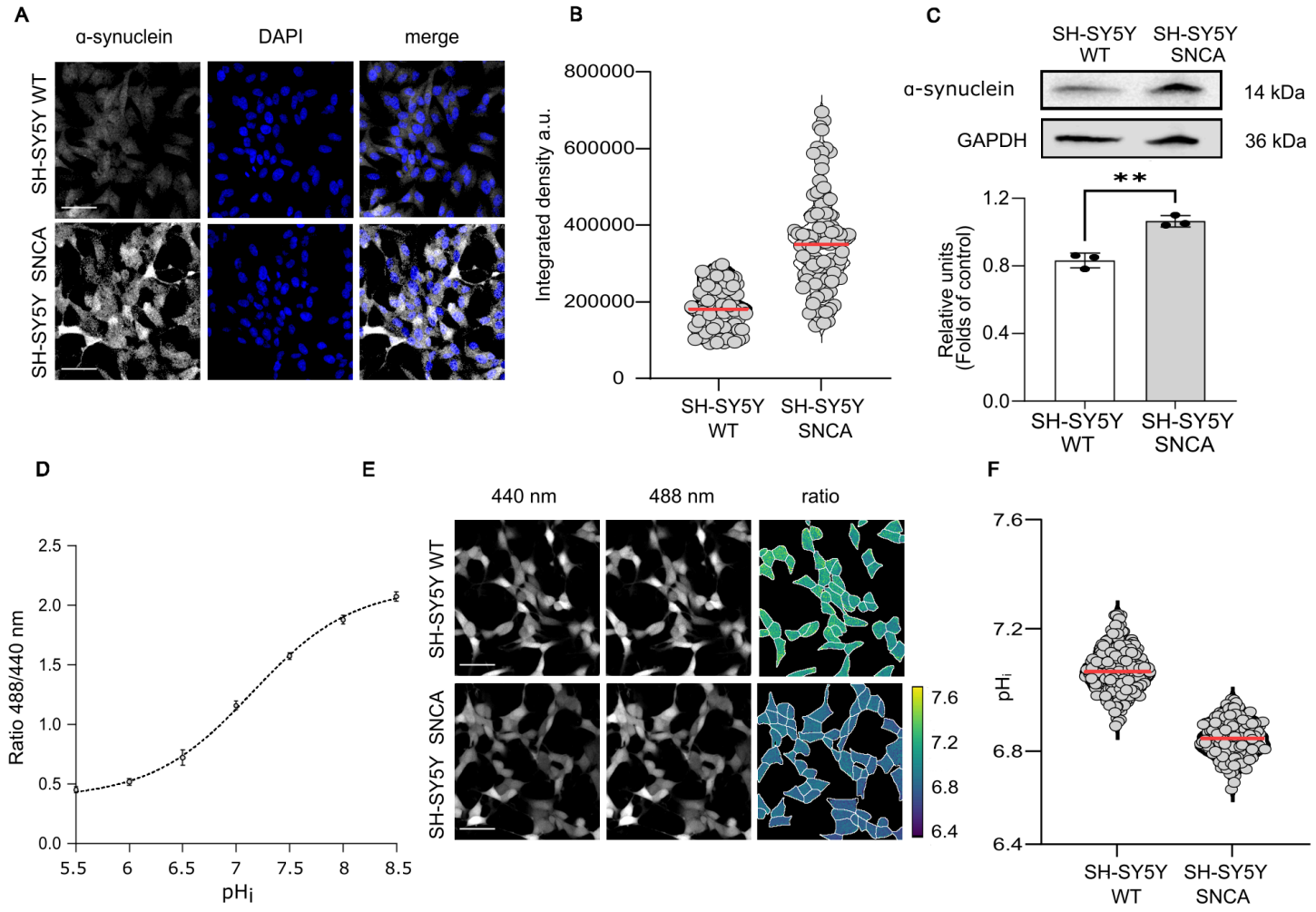


Figure 1

*α-Synuclein induces cytosolic acidification in SH-SY5Y cells. (A) Representative immunofluorescence images of --synuclein (gray) and nuclei (DAPI, blue) in SH-SY5Y wild-type (WT) and SNCA-overexpressing cells (SNCA); merged images are shown on the right. (B) Quantification of -synuclein integrated density (arbitrary units, a.u.) in WT and SNCA cells. Each dot represents a single cell; the red line indicates mean. (C) Representative Western blot of α-synuclein levels in SH-SY5Y WT and SNCA cells, with GAPDH used as a loading control. The bar graph shows relative densitometric quantification (fold of control). Data are reported as means ± SD. (D) Calibration curve of the fluorescence ratio (488/440 nm) as a function of pH_i. (E) Representative fluorescence images of BCECF dye at 440 nm and 488 nm, and corresponding 488/440 nm ratio images, in WT and SNCA cells. Pseudocolor images highlight pH_i variations. (F) Quantification of pH_i in SH-SY5Y WT and SNCA cells, calculated from the 488/440 nm ratio. Data are presented as single-cell distributions with mean. * *p < 0.01; Statistical significance was assessed using an unpaired two-tailed Student's t-test (for two-group comparisons) or one-way ANOVA followed by Tukey's post hoc test (for multiple comparisons), as appropriate. n = 6 independent experiments. *p < 0.05, **p < 0.01, ***p < 0.001.*

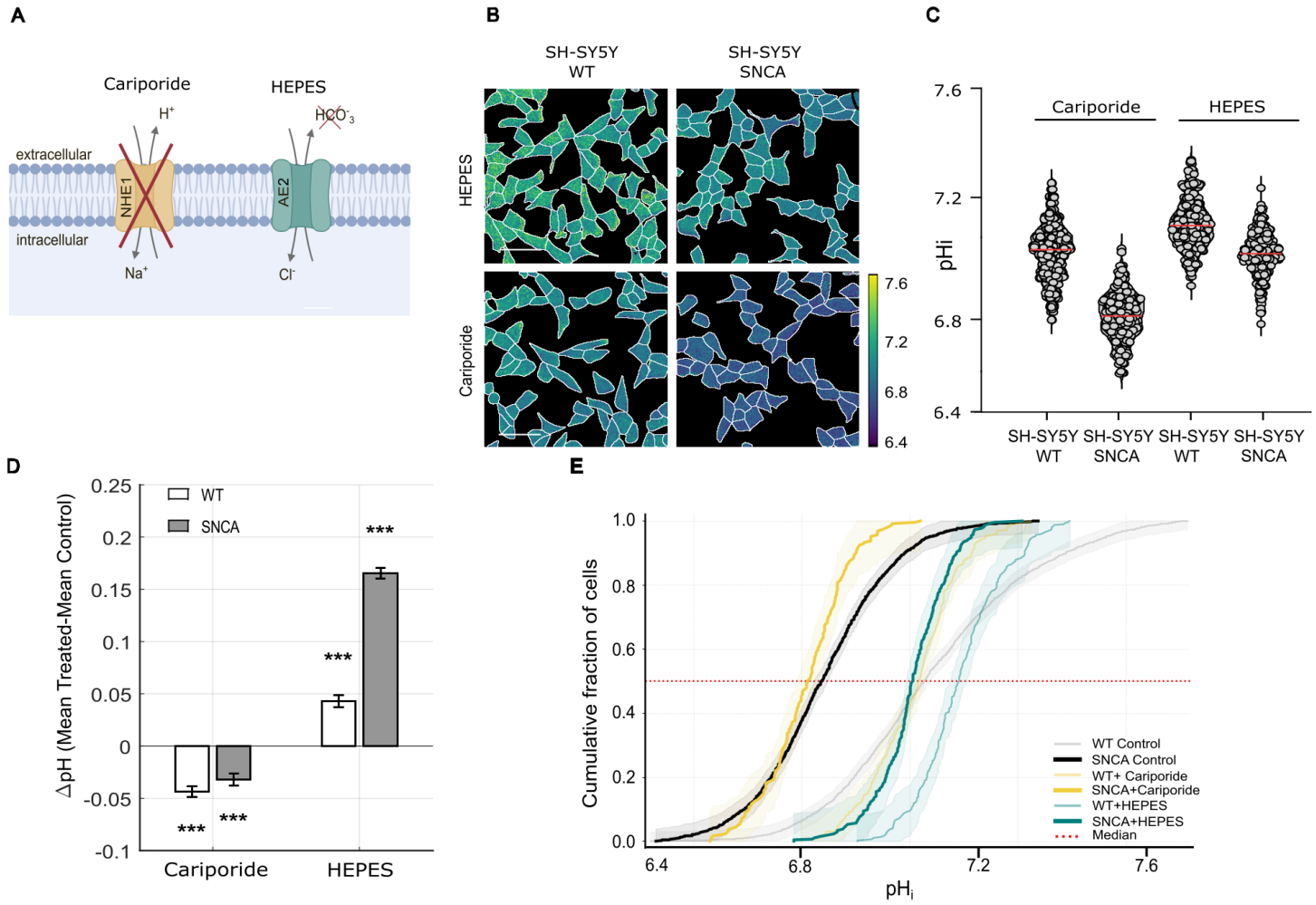


Figure 2

Differential control of intracellular pH regulation in SH-SY5Y WT and SNCA cells. A) Schematic representation of pH_i regulatory mechanisms, illustrating pharmacological inhibition of the Na^+/H^+ exchanger NHE1 by cariporide and suppression of bicarbonate-dependent anion exchange AE2 under HEPES-buffered conditions.

(B) Representative fluorescence images of BCECF dye of SH-SY5Y WT and SNCA cells acquired at 448 nm and 490 nm excitation wavelengths, together with corresponding 490/448 nm ratiometric images displayed as pseudocolor maps of pH_i under HEPES and cariporide treatments. Color scale indicates pH_i values. (C) Single-cell distribution of pH_i in WT and SNCA cells under cariporide and HEPES conditions. Each dot represents an individual cell; red lines indicate mean values. (D) Δ pH_i (delta) plot showing the change in pH_i (mean treated − mean control) in WT and SNCA cells following cariporide or HEPES treatment. Data are presented as mean ± SD ***$p < 0.001$.

(E) Cumulative distribution analysis of pH_i across experimental conditions, highlighting a leftward shift in SNCA cells under control conditions (acidification) and a pronounced rightward shift upon HEPES treatment, indicating increased dependence on bicarbonate-dependent buffering. Statistical significance was assessed using an unpaired two-tailed Student's t-test (for two-group comparisons) or one-way

ANOVA followed by Tukey's post hoc test (for multiple comparisons), as appropriate. n = 8 independent experiments. *p < 0.05, **p < 0.01, ***p < 0.001.

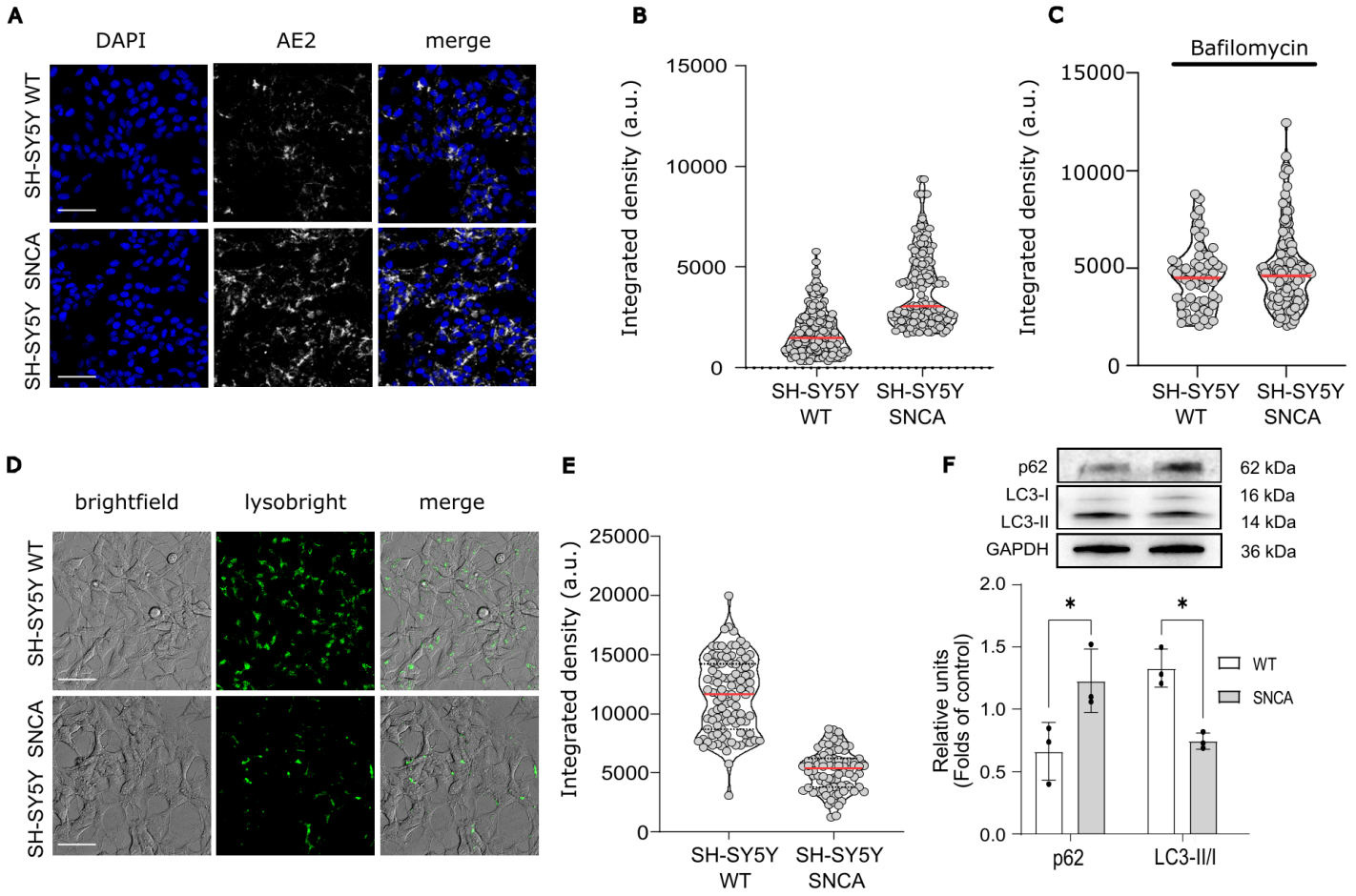


Figure 3

α-Synuclein stabilizes AE2 and disrupts lysosomal function (A) Representative immunofluorescence images of nuclei (DAPI, blue), AE2 (gray), and merged channels in SH-SY5Y WT and SNCA cells. (B) Quantification of AE2 integrated density (arbitrary units, a.u.) in WT and SNCA cells. Each dot represents a single cell; red lines indicate mean (C) Quantification of AE2 signal following bafilomycin treatment in WT and SNCA cells. (D) Representative brightfield, lysobright staining (green), and merged images in SH-SY5Y WT and SNCA cells, indicating lysosomal compartments. (E) Quantification of lysosomal signal intensity (lysobright integrated density, a.u.) in WT and SNCA cells. (F) Representative Western blot of autophagy markers (p62, LC3-I, LC3-II) in WT and SNCA cells, with GAPDH used as a loading control. Bar graphs show relative densitometric quantification (fold of control). Data are reported as means ± SD . ; Statistical significance was assessed using an unpaired two-tailed Student's t-test (for two-group comparisons) or one-way ANOVA followed by Tukey's post hoc test (for multiple comparisons), as appropriate. n = 6 independent experiments. *p < 0.05, **p < 0.01, ***p < 0.001.

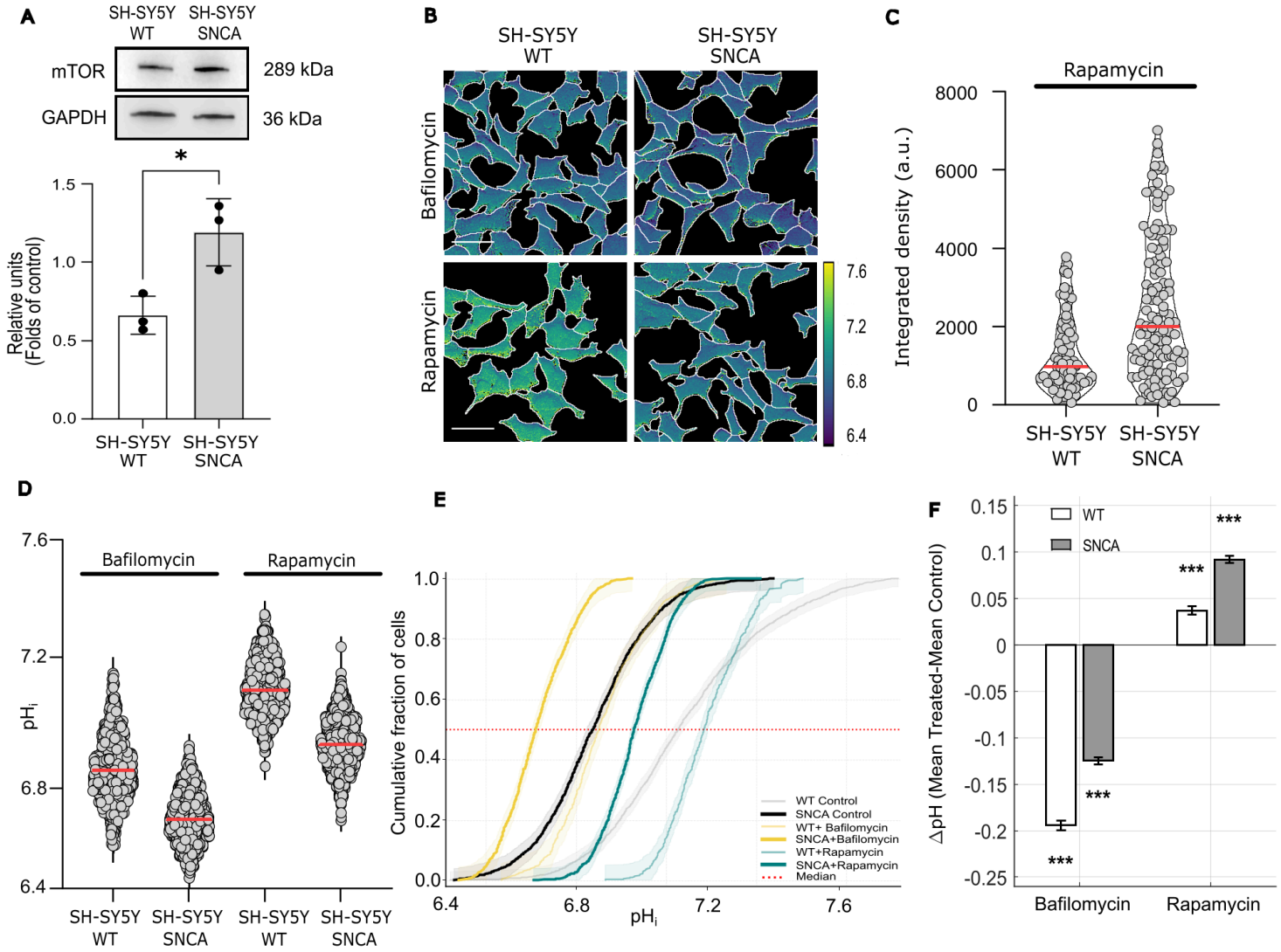


Figure 4

mTOR signaling regulates intracellular pH and lysosomal function *(A) Representative Western blot of phospho-mTOR levels in SH-SY5Y WT and SNCA cells, with GAPDH used as loading control. Quantification of band intensity (fold of control) shows increased mTOR levels in SNCA cells. Data are reported as means ± SD (B) Representative pseudocolor ratiometric images of intracellular pH (pH_i) in SH-SY5Y WT and SNCA cells treated with bafilomycin or rapamycin. Images were acquired at 448 nm and 490 nm excitation wavelengths, and corresponding 490/448 nm ratio images are displayed as pseudocolor maps. Color scale indicates pH_i values. (C) Quantification of signal intensity (integrated density, a.u.) following rapamycin treatment in WT and SNCA cells. Each dot represents a single cell; red lines indicate mean. (D) Single-cell distribution of pH_i in WT and SNCA cells under bafilomycin and rapamycin treatments. Each dot represents an individual cell; red lines indicate mean values. (E) Cumulative distribution plots of pHi across conditions. SNCA cells show a leftward shift under control conditions (acidification), which is exacerbated by bafilomycin and partially restored by rapamycin treatment. The dashed red line indicates the median. (F) Δ pH_i (mean treated − mean control) quantification in WT and SNCA cells under bafilomycin and rapamycin*

*treatments. Data are presented as mean ± SD. Statistical significance was assessed using an unpaired two-tailed Student's t-test (for two-group comparisons) or one-way ANOVA followed by Tukey's post hoc test (for multiple comparisons), as appropriate. n = 6 independent experiments. *p < 0.05, **p < 0.01, ***p < 0.001.*

Supplementary Files

This is a list of supplementary files associated with this preprint. Click to download.

- supplementary1.docx
- FigureS2WB.docx